Sargassum muticum extract based on alginate biopolymer as a new efficient biological corrosion inhibitor for carbon steel in hydrochloric acid pickling environment: Gravimetric, electrochemical and surface studies

I. Nadi, Zahira Belattmania, Brahim Sabour, Abdeltif Reani, A. Sahibed-Dine, Charafeddine Jama, Fouad Bentiss

Sargassum muticum extract based on alginate biopolymer as a new efficient biological corrosion inhibitor for carbon steel in hydrochloric acid pickling environment: gravimetric, electrochemical and surface studies

I. Nadi [a], Z. Belattmania [b], B. Sabour [b], A. Reani [b], A. Sahibed-dine [a], C. Jama [c], F. Bentiss [a,c,*]

[a] *Laboratory of Catalysis and Corrosion of Materials, Faculty of Sciences, Chouaib Doukkali University, Po Box 20, M-24000 El Jadida, Morocco*
[b] *Phycology, Blue Biodiversity & Biotechnology, P3B-LB2VE, Department of Biology, Faculty of Sciences, Chouaïb Doukkali University, Po Box 20, M-24000 El Jadida, Morocco*
[c] *University of Lille, CNRS, INRA, ENSCL, UMR 8207, - UMET - Unité Matériaux et Transformations, F-59000 Lille, France*

* Corresponding author:
E-mail address: fbentiss@gmail.com

ABSTRACT

The inhibition effect of the invasive brown seaweed *Sargassum muticum* extract (ESM), harvested from the Atlantic coast of Morocco, against the corrosion of carbon steel (CS) in 1 M HCl medium was studied for the first time using gravimetric, electrochemical and surface techniques. The methanolic crude extract of *Sargassum muticum* (ESM) is rich in alginate biopolymer. The evaluation corrosion tests showed that this algal extract acts as a good mixed corrosion inhibitor for CS substrate in 1 M HCl since inhibition efficiency of 97 % was reached with 1 g/L of ESM at 303 K. AC impedance findings showed that the seaweed extract adding in the corrosive electrolyte increases the polarisation resistance and conversely decreases the charge capacitance at the interface. Adsorption of ESM on the substrate surface followed the Langmuir adsorption isotherm. X-ray photoelectron spectroscopy analyses (XPS) demonstrated that the corrosion inhibition mechanism of CS substrate in 1 M HCl environment by the investigated algal extract is typical of the chemisorption process and the protective barrier is mainly formed by the adsorbed biological macromolecules.

Keywords: *Sargassum muticum*; Biological macromolecules; Carbon steel; HCl; Eco-friendly corrosion inhibitor; EIS; XPS.

1. Introduction

Carbon and mild steel alloys have great importance to a variety of industrial applications because of their excellent mechanical properties and its low cost. However, they are highly unstable to the aggressive environments mostly during acidic cleaning processes, which causes considerable economic losses and waste of manpower and material in the oil and gas industry [1,2]. Among kinds of anti-corrosion techniques, using inhibitors is one of the most economic and effective means for protecting against corrosion in acidification process [3-6]. Different non-organic inhibitors, such as the chromate–based compounds, have been extensively used to protect metals from corrosion attack. The use of organic compounds is also very common in industry. The known organic corrosion inhibitors are heterocyclic compounds containing a π-system and heteroatoms such as nitrogen, oxygen and sulfur [6-11]. The toxicity of these substances limits their usage as inhibitors, due to the strict environmental regulations. The urge to overcome the lacunae with environmentally friendly inhibitors has led to exploration of variety of green inhibitors [12-16]. Recently, numerous searches were led to evaluate some naturally extracted plant and algae biomass as corrosion green inhibitors for many metals in various environments [17-25]. Bio polymers present a class of efficient corrosion inhibitors, as they have good chelating ability with metal ions, cover large surface area of the surface electrode and have a good stability. Several biopolymers like lignin [26], starch [27], pectins [28], cellulose [29], polycaffiene [30], polyaspartic acid [31], chitosan [32], and polyaccharides [33] have been investigated for their anti-corrosion ability. The alginates are an anionic polysaccharides and their corrosion inhibition properties have been previously reported [34-37]. Alginates are also biocompatible, non-toxic and biodegradable, which make it usable for several industrial applications [38].

The introduced brown seaweed *Sargassum muticum* invaded the Atlantic coast of Morocco with large populations esteemed at 1,500 tons dry weight annually [39]. The brown seaweeds are generally composed of proteins, uronic acids, polysaccharides, fatty acids, mineral matter and phenolic compounds [40]. The polysaccharides are mainly found in the cellular wall matrix. The polysaccharides are present in the algal cell wall. Two forms coexist in these phaeophyceaen seaweeds: alginates and fucoidans. Alginate biopolymers are composed mainly of linear polymers of β-(1→4)-D-mannuronic (M) and α-L-guluronic (G) acids differing in terms of their proportions and linear arrangements [41,42]. Fucoidans are polymers mainly constituted by sulfated fucose [43]. Based on its content, the methanolic crude extract of *Sargassum muticum* (ESM) may be a potential candidate as eco-friendly corrosion inhibitor for CS substrate in 1 M HCl medium. Therefore, the present contribution was undertaken to assess the synergistic intermolecular effect of different constituents, containing in the natural extract, using several evaluation corrosion techniques such as weight loss, potentiodynamic polarization and AC impedance. Furthermore, we have studied the steel–ESM surface interactions in the corrosive medium using isotherm adsorption, morphological and, XPS methods.

2. Experimental details

2.1. Materials

The material, on which the review is based, is of the type carbon steel (CS), including its the composition (in wt%) of 0.230 % Si, 0.370 % C, 0.680 % Mn, 0.077 % Cr, 0.016 % S, 0.059 % Ni, 0.011 % Ti, 0.009 % Co, 0.160 % Cu and the remainder iron (Fe). Firstly, the carbon steel sheets were polished successively with a series of SiC papers (120, 400, 600 and 1200); rinsed with double-distilled water, degreased in acetone in an ultrasonic bath

immersion (for a period of 5 min), washed once again with bidistilled water and then dried at room temperature before use.

All the solvents and chemicals used in the present study were AR grade and purchased from Sigma-Aldrich Chemical Company and used without further purification.

The biomass of the invasive brown seaweed *Sargassum muticum* was harvested at low tide from the Northwestern Atlantic coast of Morocco at the south of El Jadida city. The algal samples were washed in running tap water and then with distilled water to eliminate impurities, after which they were dried in an oven at 333 K then grounded to powder and mixed. 300 g of powdered alga was refluxed with methanol for 6 h. The resulting solution was evaporated yielding 44.6 g of solid extract (yield = 14.9 %). A suitable quantity of the obtained solid extract was dissolved in 1 M HCl solutions to get desired concentrations of inhibitor solution ranging from 0.5 to 1.5 g/L. 1 M HCl solutions were prepared by dilution of an analytical reagent grade 37 % HCl with double distilled water.

The analysis of the main chemical components of the used biomass of *Sargassum muticum* revealed that alginate biopolymer is the major constituent of this alga reaching 25.62 ± 1.4 % on dry weight basis (dw) [44], followed by soluble carbohydrates and protein accounting for 15.58 % ± 0.16 and 9.73% ± 0.27 % dw, respectively [45]. Furthermore, *Sargassum muticum,* as the most brown algae, produce phenolic compounds called phlorotannins (phloroglucinol-like molecules), representing around 1.7 ± 0.12 % dw [46]. This invasive species contains also about 5.48 ± 0.52 µg/g of fatty acid methyl esters, with the arachidonic (C20:4) and linoleic (C18:2) acids as the most characteristic polyunsaturated fatty acids [47]. Schematic presentation of the macromolecules containing in the ESM is shown in Fig. 1.

2.2. Corrosion tests

Gravimetric experiments have been performed in accordance with the standard method "A.S.T.M G1-03" described beforehand [48]. Firstly, the CS specimens (1.5 × 1.7 × 0.3 cm) were weighed and immersed in 1 M HCl electrolyte lacking adding and with adding various concentrations of ESM at definite time interval of 6 h at 303 K. After exposure period, the steel specimens were withdrawn, carefully rinsed with distilled water, ultrasonically cleaned in acetone, dried at and then weighted again. The tests were performed in triplicate and the mean value of weight loss was obtained. The corrosion rate (C_R), expressed in mils per year (mpy), and the inhibition efficiency, (η_{WL}), in percent (%), were determined as described previously [49]

DC measurements were performed in a conventional three-electrode cylindrical Pyrex glass cell using Solartron Instruments SI 1287 potentiostat. A platinum electrode as the counter electrode and a saturated calomel electrode (SCE) as the reference electrode. The working electrode (WE) in the form of disc cut from the tested carbon steel has a geometric area of 1 cm^2 and embedded in polytetrafluoroethylene (PTFE). A period of 1 h was allowed for the electrochemical system to reach the steady open circuit potential (OCP) before each electrochemical measurement. DC measurements were scanned from cathodic to the anodic direction, $E = E_{corr} \pm 200$ mV, with a scan rate of 0.5 mV s^{-1}. CorrWarr 2.80 software was used to run the tests and to collect the experimental data. AC impedance studies were carry out in a polymethyl methacrylate (PMMA) cell with a capacity of 1000 ml at temperature of 303 ± 1 K, using a thermostat. The working electrode was prepared from a square sheet of CS such that the area exposed to solution was 7.55 cm^2. The EIS measurements were realized after 6 h of immersion in the frequency interval of 10^5 Hz to 0.01 Hz at E_{ocp} with an amplitude of 10 mV. The detailed DC and AC electrochemical procedures were previously described [10].

2.3. Surface analyses

Scanning Electron Microscopy (JEOL 5300) was employed in assessing the surface quality of CS substrate without and with addition of ESM.

X-ray photoelectron spectroscopy (XPS) spectra were registered using XPS KRATOS, AXIS UltraDLD spectrometer Thermo Scientific K-Alpha XPS system. The XPS experiment and data treatment were made according to the same procedures previously described [50].

3. Results and discussion

3.1. Weight loss study

The inhibition properties of the ESM towards the steel corrosion was analysed using the gravimetric study by introducing various concentrations of ESM to the corrosive solution. From the gravimetric data, C_R and η_{WL} values of the CS substrate after 6 h immersion period in 1 M HCl medium at 303 K were calculated; the results are listed in Table 1. It's clear that an obvious decrease is shown in C_R with increasing of the inhibitor concentration (C_{inh}), probably due to the adsorption of the ESM molecules on the CS surface. Conversely, this suggest an increment in the surface coverage and therefore an increase in the inhibition efficiency was observed. Indeed, the upsurge in η_{WL} from 73.6 to 96.6 % as the ESM concentration increased from 0.5 to 1.5 g/L can be caused by the result of enhanced surface coverage at higher concentrations through the adsorption of phyotochemical constituents of the ESM extract on the CS surface. The maximum inhibition efficiency was attained at 1.5 g/L concentration of ESM and no appreciable change was noticed on further addition of inhibitor. Indeed, the ESM adsorption at the electrode surface can be done in two ways, physisorption and/or chemisorption. The protonation of ESM molecules in HCl solution allowed to form the

cation-ionic forms of ESM and therefore these latter adsorb at the substrate surface through the adsorbed chloride ions [51]. The neutral ESM molecules can be also adsorbed on substrate surface by forming the chemical bonds between the *d*-orbital of iron atoms and the lone sp^2 electron pairs present on the heteroatoms (O) and π-orbitals in aromatic groups. This behaviour induces the displacement of water molecules from the metal surface and the blocking the active sites in the CS surface and hence decreasing the C_R of CS substrate [52]. Besides, the inhibitive nature of ESM may be attributed to the synergistic intermolecular effect of the different active constituents present in this seaweed extract. The large size of constituent's biological macromolecules, such as the alginates, can be benefit to greater coverage of the metallic surface [53,54] and may play the role of an effective barrier from the acidic medium, contributing thus to the high inhibitive performance of ESM.

3.2. Polarization study

The open circuit potential (E_{OCP}) for the studied samples was monitored until the steady state condition was obtained at the surface of CS before each electrochemical measurement. The time-dependent variation of E_{OCP} of CS electrode in 1 M HCl solution containing various concentrations of ESM at 303 K is presented in Fig. 2. The analyse of this figure shows clearly that the initial potential shifted over time towards negatives value for all concentrations and gradually remains constant. In the uninhibited solution, the E_{OCP} value gradually decreases with time, which may be attributable to the corrosion occurred on the surface. After about 15 min of immersion time, the E_{OCP} value stabilizes at around -0.485 V/SCE, which corresponds to the free corrosion potential of the bare metal. The introduction of ESM inhibitor in the corrosive medium leads the shift of the E_{OCP} towards more positive values, probably due to the adsorption of seaweed extract on the CS surface and therefore the improvement its corrosion resistance in hydrochloric acid pickling solution. It is, moreover,

noteworthy there was no a specific relation between the potential shift of E_{OCP} and inhibitor concentration.

The inhibition performance of the investigated seaweed extract (ESM) on the corrosion process of CS in 1 M HCl medium at 303 K has also been performed by potentiodynamic polarization (PDP) and the obtained Tafel plots are presented in Fig. 3. The calculated electrochemical parameters such as corrosion current density (i_{corr}), corrosion potential (E_{corr}), cathodic and anodic Tafel slopes (β_c and β_a), as well as inhibition efficiency, $\eta_{Tafel}(\%)$, were summarized in Table 2. The data were fitted using the Tafel-LEV method using CorrView 2.80 software (Scribner Associates, Inc.). The $\eta_{Tafel}(\%)$ values were determined as described previously [54].

Careful inspection of Fig. 3 reveals that the cathodic current-potential curves give rise to the parallel Tafel lines, which indicate that hydrogen reduction reaction is activation controlled and that the addition of ESM does not modify the mechanism of this process [54]. However, the anodic curves of carbon steel in 1 M HCl in the presence of the algal extract show that this compound has no effect at potential higher than -0.3 V/SCE. At this potential it appears there is a significant steel dissolution leading to desorption of the inhibiting layer. In that event, the desorption rate of the tested inhibitor is higher than its adsorption rate [54]. Also, Fig. 3 shows that both the anodic as well as cathodic curves were hindered after adding the ESM inhibitor to the corrosive solution. The investigated seaweed extract decreases the current densities, and its effect becomes more efficient when the ESM concentration increases. This is totally attributed to the reduction in both anodic and cathodic reactions on the CS surface. Hence, the steel dissolution and hydrogen reduction were significantly reduced at its corresponding reaction sites [55]. Usually, if the shift of E_{corr} is less than 85 mV compared to the uninhibited solution, the inhibitor acts as a mixed type [56,57]. the E_{corr} shifted negatively after adding ESM, with the maximum displacement at 27 mV as shown in

Fig. 7. This shift was less than 85 mV, which is the characteristic feature of mixed type inhibitive nature, with predominant cathodic effectiveness. The polarization results in Table 2 reveals a significant reduction of i_{corr} upon addition of ESM compared with that of the blank electrolyte and η_{Tafel} increased with increasing of ESM concentration. The maximum corrosion inhibition (90.9 %) attained at 1.5 g/L with lesser corrosion current value of 65 μA cm^{-2}, indicating the effective inhibition effect of ESM against acid steel corrosion. The polarisation findings are in the same trend with the gravimetric results. Besides, the cathodic Tafel slope (β_c) decreased after ESM addition to the corrosive medium, indicating that the investigated seaweed extract have a direct influence on the kinetics of hydrogen evolution [58]. Also, the β_a values decreased after addition of ESM indicating that that the anodic reaction is affected by the presence of the green inhibitor [59]. This behaviour suggested the formation of a protective film due to adsorption of the ESM molecules on the metal surface decreasing the active sites of the CS surface. Moreover, the abundance of oxygen atoms in the alginate components (hydroxyl and carboxylate groups) can facilitate the formation of ESM–Fe(II) complex, forming a protective barrier which prevents the CS dissolution.

3.3. AC impedance study

The AC impedance method can provide extensive information on the kinetics of the electrode processes as well as on the properties of the steel surface [60]. The impedance response of steel in inhibited and inhibitor-free solutions are graphically represented as Nyquist and Bode (modulus, and phase angle) diagrams (Figs. 4 and 5). From Fig. 4, a slightly depressed capacitive loop was observed for the metal in the blank acid solution, corresponding to one time constant in Bode-phase diagram as shown in Fig. 5b. The adding of the seaweed extract does not modify the profile of Nyquist plots that are depressed semicircles. This behaviour suggests that the corrosion of CS is mainly charge transfer-based

without alteration in the mechanism of the corrosion reaction [61,62]. However, a small second capacitive loop at low frequencies was observed in the presence of high concentrations of ESM (1 and 1.5 g/L) (see Fig. 4) and can be attributed to the adsorption of inhibitor molecules on the metal surface and/or all other accumulated kinds at the metal/solution interface (inhibitor molecules, corrosion products, etc) [63]. For the uninhibited and inhibited cases, the deviation from the perfect semi-circular shape, known as the frequency dispersion of the interfacial impedance, might result from roughness as well as other forms of interfacial phenomena [64,65]. Indeed, the slope (*s*) values of the Bode-modulus plots (Fig. 5a) for intermediate frequency values were not equal to -1 (ideal capacitor); they were -0.59 for uninhibited solution and -0.65, -0.71, -0.83, and -0.87 after addition of 0.5, 0.75, 1 and 1.5 g/L of ESM, respectively. This can attributed to the frequency dispersion of interfacial impedance.

The diameter of the Nyquist capacitive loop increased as a result of increasing the charge transfer resistance and that happens by increasing the ESM concentration, meaning higher corrosion resistance. In the same way, the global impedance modulus values at 0.01 Hz ($|Z|_{0.01HZ}$) were 25.8 Ω cm^2 for 1 M HCl lacking adding and 90.74, 282.21, 734.79, and 988.28 Ω cm^2 with adding 0.5, 0.75, 1 and 1.5 g/L of ESM, respectively (Fig. 5a). Furthermore, the maximum phase angles (α_{max}) of the uninhibited and inhibited solutions are -52.05°, -52.73°, -61.82°, -71.48° and -73.53°, respectively (Fig. 5b). The values of phase angle and impedance magnitude show an increment with ESM concentration, which indicates better protection behaviour of the seaweed extract with higher concentrations. The gradual approach of the α_{max} values to the ideal capacitive behaviour (-90°) may be explained by slowing down of the rate of dissolution with time which reflects the inhibitive action of ESM. The protective inhibitor layer adsorbed on the CS surface behaves as an active barrier to the aggressive attack by the corrosive acid medium [11,52].

EIS parameters derived by fitting the impedance plots with the electrochemical equivalent circuit (EEC), shown in Fig. 6, are listed in Table 3. The used EEC consists of an electrolyte resistance (R_s) in series with a constant phase element (CPE) in parallel to the polarization resistance ($R_{p)}$, where R_p comprises the charge transfer resistance (R_{ct}), the resistance of inhibitor film (R_f), and all other accumulated species (R_a) ($R_p = R_{ct} + R_f + R_a$) [65]. The ideal capacity of the double layer capacitance (C_{dl}) was substituted by CPE in the ECC obviate the deviation resulting from the frequency dispersion [66]. The impedance of CPE (Z_{CPE}) and C_{dl} can be described as follows [66]:

$$Z_{CPE} = Q^{-1}(i\omega)^{-n} \quad (1)$$

$$C_{dl} = (QR_p^{1-n})^{1/n} \quad (2)$$

where Q is the magnitude of CPE (in Ω^{-1} s^n cm^{-2}), i is the imaginary root ($i^2 = 1$), w is the angular frequency in (rad s^{-1}) and n is an empirical exponent ($0 \leq n \leq 1$) which measures the deviation from the ideal capacitive behaviour [11]. In this case, the relaxation time constant (τ) is calculated by the following formula:

$$\tau = C_{dl} R_p \quad (3)$$

The inhibition efficiency in the case of AC impedance study, $\eta_Z(\%)$, was computed from R_p values using the Eq. (4) [67]:

$$\eta_Z(\%) = \frac{R_{P(i)} - R_p}{R_{P(i)}} \times 100 \quad (4)$$

where R_p and $R_{p(i)}$ are the polarization resistance values without and with addition of ESM, respectively. The accuracy of the EIS measurements can be verified from the strong agreement between the experimental plots and fitting lines (Fig. 7), as well as the values of goodness of fit in Table 3. Indeed, the goodness of fit chi-squared (χ^2) values are of the order of 10^{-4} (Table 3), suggesting the validity of the proposed circuit (in theory the lower value of χ^2 shows that the fitted data agrees well with the experimental data). A typical example of the fitted diagrams (Nyquist and Bode) with the used EEC, presented in Fig. 7, indicated that the used model is well representative of the investigated system (CS / 1 M HCl / ESM inhibitor). Based on the Table 3, the obtained results revealed a significant enhancement in polarization resistance (R_p) with increase in the seaweed extract concentration, therefore $\eta_Z(\%)$ increased and reached a maximum of 97.7 % at 1.5 g/L of ESM. This is consistent with the obtained data by weight loss and PDP measurements. The biological molecules of phytochemical components of ESM are adsorbed on the exposed CS surface and block therefore the active sites which are available for corrosive dissolution whereby causing an increment in the R_p values which is correlated with corrosion inhibitive performance. However, a substantial decrease in C_{dl} with ESM concentration was observed, may be owing to the decrease in the dielectric constant through replacement of the pre-adsorbed water molecules [68]. Diminution in dielectric constant intensifies the adsorption ability of the extract molecules. This marks in greater coverage and better protection of the metal against dissolution, confirmed by the increase of the inhibition performance with the ESM concentration as presented in Table 3. It is worth pointing that the rise in the deviation parameter (n) values after the inhibitor addition, which can be related to a decrease of surface inhomogeneities caused by adsorption of the seaweed extract components on CS surface [69]. Furthermore, the value of τ increases with ESM content, meaning a slow adsorption process [70].

The use of the marine algal extracts [71-77] and alginate based polymers [35,36,78] as corrosion inhibitors for steel in 1 M HCl medium have been reported by several authors. Based on the analysed literature related to our work, relevant informations were found, whose data are summarized in Table 4. From this Table, it is evident that our crude extract of *Sargassum muticum* (ESM) shows higher inhibition efficiency in comparison to the other algal extracts and alginate based inhibitors, even though the immersion time in the corrosive medium is much longer (6 h). In conclusion, *Sargassum muticum* extract possesses good corrosion inhibition properties for carbon steel in acidic environment.

3.4. Surface and isotherm adsorption studies

The SEM micrographs of the surfaces of CS samples before and after adding of the seaweed extract in corrosive medium are presented in Figs. 8 a-c. The comparison of SEM micrographs is carried out at same magnification in order to see the changes happened during the corrosion process. On the polished CS surface before acid immersion, the parallel abrading scratches are clearly observed in Fig. 8a. After exposure to 1 M HCl medium, the SEM micrograph in Fig. 8b shows that the CS surface was strongly damaged, due to rapid corrosion attack in the absence of ESM inhibitor. However, relatively smoother surface with few small notches are seen after adding of the ESM in the pickling solution (Fig. 8c). The later may be explained by formation of adsorbed ESM layer on the substrate surface.

Fundamental information on the adsorption of inhibitor on metal surface can be described by adsorption isotherm [62]. Several isotherms including Langmuir, Frumkin, and Temkin, isotherms are conducted to fit the experimental data. The adsorption isotherms can be expressed in the following equations [79]:

$$\frac{C_{\text{inh}}}{\theta} = \frac{1}{K_{\text{ads}}} + C_{\text{inh}} \qquad \text{(Langmuir)} \qquad (5)$$

$$\exp(-2a\theta) = K_{ads} C_{inh} \quad \text{(Temkin)} \tag{6}$$

$$\left(\frac{\theta}{1-\theta}\right)\exp(2a\theta) = K_{ads} C_{inh} \quad \text{(Frumkin)} \tag{7}$$

where θ is the fractional surface coverage; a is the molecular interaction constant; and K_{ads} is the equilibrium constant of the adsorption process. The values of θ can be easily determined by from AC impedance results by $\eta_Z(\%) / 100$ [80]. The different isotherm plots are presented in Fig. 9. Based on the values of correlation coefficient (R^2), it is evident that the Langmuir was the best fit model for the adsorption of ESM molecules on the CS surface for which the R^2 value was found to be close to 1 (0.99), while its values are equal to 0.79 in the case of Temkin and to 0.82 in the case of Frumkin isotherm. The Langmuir isotherm exhibits single-layer adsorption characteristic, assuming that no interaction between the adsorbed molecules on the steel surface [81]. However, this behaviour subsists speculative in the case of plant extracts, simply because to the intermolecular effects (electronic and steric) of different active constituents present in the investigated extract.

The standard Gibbs free energy of adsorption, ΔG°_{ads}, is related to K_{ads} according to [82]:

$$K_{ads} = \frac{1}{C_{H_2O}} \exp\left(\frac{-\Delta G^{\circ}_{ads}}{RT}\right) \tag{8}$$

where R is the universal gas constant, T the thermodynamic temperature and the concentration of water in the solution is 1000 g/l. Based on the literature, ΔG°_{ads} values around –20 kJ mol^{-1} or less negative, the adsorption is assumed as physisorption; while those around –40 kJ mol^{-1} or more negative, the adsorption is typical of chemisorption [83,84]. Unfortunately, the molecular weight of the investigated algal extract (ESM) is not known, and

therefore the calculation of the ΔG°_{ads} value in this case is not possible. This conclusion is in agreement with those described previously in the case of some plant extracts used as corrosion inhibitors [85-88].

The XPS analysis was consequently performed to obtain some information's on the surface coverage of ESM after immersion in 1 M HCl medium and the obtained XPS wide-scan (survey) spectrum is shown in Fig. 10. Besides, the obtained high-resolution peaks for C 1s,

O 1s and Fe 2p core levels, through a deconvoluted fitting procedure using the CASA XPS software, were given in Fig. 11 and the corresponding data are summarised in Table 5.

The C 1s peak deconvolution may be fitted into three components located at 285.0, 286.4, and 288.7 eV as shown in Fig. 11 and Table 5. The first component presents the largest contribution (53 %) and can be attributed to contaminant hydrocarbons and to the C–C, C=C and C–H bonds in the ESM molecules [67]. The second component is mainly ascribed to the C–N, C=N bonds, and C–O in ether, in hydroxyl and / or in carboxylate groups (O=C–O^-), present in biological molecules of the seaweed extract [67,89]. The last and less intense component (15 %) can be associated to shake-up satellite due to π-π* transitions in aromatic rings and also to the presence of carboxylate groups [89]. The presence of different carbon environments, especially of the carboxylate groups, demonstrates that the seaweed extract molecules are adsorbed on the steel surface. Comparison of the component shape of C 1s peak of ESM extract powder (Fig. 12a) and ESM-treated steel (Fig. 12b) was carried out in order to gain some additional insight into changes in relative proportion of different components and their binding energies. The C 1s peak spectra of both cases are very similar; three components at the same binding energies as described above, with slight variation in the component contribution. Indeed, a significant increase in the contribution of the component at high binging energy is observed in the case of ESM-treated steel sample, probably due to the

adsorption of the ESM molecules on the steel surface through the carboxylates group of alginate molecules. The comparison result may suggest that the steel surface is entirely covered with ESM molecules. In order to confirm this assumption, XPS surface elemental analyses of ESM extract and ESM-treated steel samples were performed and given in Table 5. In both cases, the sum of the atom concentrations was normalized to 100% in order to easily compare surface concentrations for the different elements. Inspection of the obtained results shows that the atom concentration values of C are about 68% in both cases and the surface distribution of O and N concentrations generally followed similar trends for ESM powder and ESM treated-steel. On the other hand, the C and O represent the main elements present in both samples, while the Fe amount is very low in the case of ESM treated-steel surface (Table 6), suggesting therefore that the inhibitive layer formed in the presence of ESM extract is thick.

Yet, the comparison of component shape of O 1s peak of ESM extract (Fig. 12a) and ESM-treated steel (Fig. 12b) showed that the both spectra are very different. Indeed, the O 1s spectrum in the case of ESM extract is composed of two peaks at 532.1 and 533.2 eV. The first one corresponds to oxygen in the O–H and in O–C (ether and / or hydroxyl) and the second one, which presents the most contribution (78 %), can be attributed to the presence of COO^- (carboxylate groups) of alginates in the seaweed extract (Fig. 1). After immersion in 1 M HCl solution containing ESM, the O 1s spectrum for CS surface can be resolved into three components (Fig. 11, Table 5). The first one, at 530.1 eV, is associated to O^{2-}, and in principle may be related to oxygen double bonded to Fe^{3+} in the iron oxide (Fe_2O_3) [90]. The second component, located at. 532.6 eV, is the most intense one (66 %) and can be assigned to combined effects of singly bonded oxygen (–O–). Indeed, this component can be partly ascribable to OH^- of hydrous iron oxides, such as FeOOH [90] and mainly assigned to singly bonded oxygen (–O–) in O–H, in C–O (ether and / or hydroxyl) [89] and to adsorbed COO^-

(carboxylate groups) of alginates in the seaweed extract molecules. It is clear that this component slightly shifted to lower binding energy side (ΔE_b = 0.6 eV) compared to that one observed in the case of ESM extract (Fig. 12). This behaviour may be explained by the coordination of the negative oxygen of adsorbed carboxylate groups (COO^-) with the Fe atom of steel surface, i.e. formation of COO–Fe bond complex which cancels the negative polarization of the oxygen atom, and therefore a core-level chemical shift to lower binding energy is produced. It has been reported that the carboxyl oxygen plays the fundamental role during the interaction between alginic acid and metal ions [91]. The last component at 533.3 eV can be attributed to the non-adsorbed carboxylate groups of ESM molecules [83] and to oxygen of adsorbed water [92], which remained on the surface after drying the sample. Moreover, the XPS surface elemental analyses show that the atom concentration of O is slightly high in the case of ESM-treated steel sample (27.86 %) compared to that of ESM extract powder (21.03 %) (Table 6). This difference is due to the formation of oxidized species (Fe_2O_3, FeOOH) in the corrosive solution (1 M HCl) and therefore ESM molecules are incorporated into the oxide/hydroxide iron layer formed on the CS surface.

The high resolution Fe $2p_{3/2}$ XPS spectrum can be deconvoluted in three components (Fig. 11, Table 5). The first one, at 706.8 eV, is attributed to metallic iron [93], while the second at 710.3 eV is assigned to Fe^{3+} [94,95], associated to the presence of Fe_2O_3 and FeOOH, as shown in the O 1s spectrum (Fig. 11). The last component at 714.4 eV can be attributed to the satellite of Fe(III) [96] and also can be related to the presence of $FeCl_3$ on the CS surface due to the testing medium (HCl) [97]. This assumption is confirmed by the detection of the Cl signal in the survey spectrum (Fig. 10).

Based on the XPS data analysis, it can be suggested that the chemical interactions (chemisorption) were occurred between CS surface and ESM extract molecules. The use of ESM extract in the corrosive solution promotes the formation of the stable metal-organic

complex (ESM/Fe), through the carboxylate groups of alginate molecules, and an insoluble oxide layer (Fe_2O_3, FeOOH). Indeed, the alginates are the major constituent of this alga (25.62 %), their adsorption on the steel surface allows the formation of an inert barrier that surely isolates the CS surface from the HCl medium attack due to their high hydrophobicity [37] and promotes the steady state formation and growth of a well-developed and protective corrosion product layer on the CS surface.

Conclusions

The invasive brown seaweed *Sargassum muticum* extract (ESM), based on the alginate biopolymer, presented a good skill to inhibit the corrosion process of carbon steel (CS) substrate in 1 M hydrochloric acid solution by working as mixed kind inhibitor. The inhibition efficiency of ESM increased with inhibitor concentration attenuating a value up to 97% at 1 g/L. The AC impedance results demonstrated the decrease of C_{dl} and increase of R_p values when adding ESM, due to the adsorption of extract algal molecules on the CS surface according to Langmuir isotherm model. XPS analysis demonstrated that the adsorption mechanism of ESM on CS surface in 1 M HCl solution is mainly due to chemisorption, which revealed the protective layer formed from metal–inhibitor on the CS surface. The excellent corrosion inhibition properties of the investigated methanolic crude extract of *Sargassum muticum* (ESM), with both economic and environmental benefits as well as high availability, permit to consider this product as a new renewable and eco-friendly promising corrosion inhibitor for CS substrate in acidic pickling media.

Acknowledgments

The authors are greatly thankful to the CUR CA2D of Chouaib Doukkali University for fund and support.

References

[1] M. Yunovich, N.G. Thompson, Concr. Int., 25 (2003) 52–57.
[2] S.T. Zhang, Z.H. Tao, W.H. Li, B.R. Hou, Appl. Surf. Sci. 255 (2009) 6757–6763.
[3] S. Pehkonen, S. Yuan, Tailored Thin Coatings for Corrosion Inhibition Using a Molecular Approach, 1st Edition, Academic Press, Elsevier, 2018.
[4] Y.I. Kuznetsov, Organic Inhibitors of Corrosion of Metals, Springer, 1996.
[5] M. Aliofkazraei, Developments in Corrosion Protection, In Tech, ISBN 978-953-51-1223-5, 2014.
[6] M. Goyal, S. Kumar, I. Bahadur, C. Verma, E.E. Ebenso, J. Mol. Liq. 256 (2017) 927–942.
[7] S. Hooshmand Zaferani, M. Sharifi, D. Zaarei, M.R. Shishesaz, J. Environm. Chem. Eng. 1 (2013) 652–657.
[8] B.N. Popov, Corrosion inhibitors, In Corrosion Engineering, Chapter 14, Elsevier, 2015, pp. 581–597.
[9] M. Finšgar, J. Jackson, Corros. Sci. 86 (2014) 17–41.
[10] V.S. Sastri, Types of corrosion inhibitor for managing corrosion in underground pipelines, in: M.E. Orazem (Ed.), Underground Pipeline Corrosion, Woodhead Publishing, 2014, pp. 166–211.
[11] F. Bentiss, M. Outirite, M. Traisnel, H. Vezin, M. Lagrenée, B. Hammouti, S.S. Al-Deyab, C. Jama, Int. J. Electrochem. Sci. 7 (2012) 1699–1723.
[12] P.B. Raja, A.K. Qureshi, A. Abdul Rahim, H. Osman, K. Awang, Corros. Sci. 69 (2013) 292.
[13] H. Gerengi, H.I. Sahin, Ind. Eng. Chem. Res. 51 (2012) 780–787.
[14] L. Li, X. Zhang, J. Lie, J. He, S. Zhang, F. Pan, Corros. Sci. 63 (2012) 82–90.
[15] J.C. da Rocha, J.A. Da Cunha Ponciano Gomes, E. D'Elia, Corros. Sci. 52 (2010) 2341–2348.
[16] G. Gunasekaran, L.R. Chauhan, Electrochim. Acta 49 (2004) 4387–4395.
[17] P.B. Raja, M.G. Sethuraman, Mater. Lett. 62 (2008) 113–116.
[18] N. Poongothai, T. Ramachanderan, M. Natesan, S.C. Murugavel, Mater. Perform. 48 (2009) 52–56.
[19] M. Gopiraman, P. Sakunthala, D. Kesavan, V. Alexramani, I.S. Kim, N. Sulochana, J. Coat. Technol. Res. 9 (2012)15–26.
[20] A. Singh, E.E. Ebenso, M.A. Quraishi, Int. J. Corros. 2012 Article ID 897430 (and references therein).
[21] G. khan, K.M.S. Newaz, W.J. Basirun, H.B.M. Ali, F.L. Faraj, G.M. Khan, Int. J. Electrochem. Sci. 10 (2015) 6120–6134
[22] C. Verma, E.E. Ebenso, I. Bahadur, M.A. Quraishi, J. Mol. Liq. 266 (2018) 577–590.
[23] C. Kamal, M. G. Sethuraman, Mater. Corros. 65 (2014) 846–854.
[24] Y. Abboud, A. Abourriche, T. Ainane, M. Charrouf, A. Bennamara, O. Tanane, B. Hammouti, Chem. Eng. Commun. 196 (2009) 788–800.
[25] C. Kamal, M. G. Sethuraman, Res. Chem. Intermed. 39 (2013) 3813–3828.
[26] Y. Ren, Y. Luo, K. Zhang, G. Zhu, X. Tan, Corros. Sci. 50 (2008) 3147–3153.
[27] M. Mobin, M.A. Khan, M. Praveen, J. Appl. Polym. Sci. 121 (2011) 1558–1565.
[28] M.V. Fiori-Bimbi, P.E. Alvarez, H. Vaca, C.A. Gervasi, Corros. Sci. 92 (2015) 192–199.
[29] V. Rajeswari, D. Kesavan, M. Gopiraman, P. Viswanathamurthi, Carbohyd. Polym. 95 (2013) 288–294.
[30] F.S. de Souza, A. Spinelli, Corros. Sci. 51 (2009) 642–649.
[31] B. Qian, J. Wang, M. Zheng, B. Hou, Corros. Sci. 75 (2013) 184–192.
[32] Y. Sangeetha, S. Meenakshi, C. Sairam Sundaram, Int. J. Biol. Macromol. 72 (2015) 1244–1249.
[33] I.O. Arukalam, I.C. Madufor, O. Ogbobe, E.E. Oguzie, Brit. J. Appl. Sci. Technol. 4 (2014) 1445–1460.
[34] S.A. Umoren, U.M. Eduok, Carbohyd. Polym. 140 (2016) 314–341.
[35] S.M. Tawfik, RSC Adv. 5 (2015) 104535–104550.
[36] Y. Sangeetha, S. Meenakshi, C.S. Sundaram, J. Appl. Polym. Sci 133 (2016) 43004–43009.
[37] I.B. Obot, I.B. Onyeachu, A.M. Kumar, Carbohyd. Polym. 178 (2017) 200–208.
[38] F.L. Mi, H.W. Sung, S.S. Shyu, Carbohyd. Polym. 48 (2002) 61–72.

[39] S. Elatouani, F. Bentiss, A. Reani, R. Zrid, Z. Belattmania, L. Pereira, A. Mortadi, O. Cherkaoui, B. Sabour, Phycol. Res. 64 (2016) 185–193.
[40] D. Maureen, P. Maya, D. Philippe, V. Stiger-Pouvreau, B. Gilles, B. Nathalie, V. Laurent, J. Anal. Bioanal. Sep. Tech. 2 (2017) 1–10.
[41] O. Smidsrød, B.E. Christensen, Molecular structure and physical behaviour of seaweed colloids as compared with microbial polysaccharides. In: Guiry MD & Blunden G. (Eds.), Seaweed Resources in Europe, uses and potential. John Wiley & Sons, United States, 1991, pp. 185–217.
[42] K.I. Draget, C. Taylor, Food Hydrocolloid. 25 (2011) 251–256.
[43] E.M. Balboa, S. Rivas, A. Moure, H. Dominguez, J.C. Parajo, Mar. Drugs 11 (2013) 4612–4627.
[44] S. El Atouani, F. Bentiss, A. Reani, R. Zrid, Z. Belattmania, L. Pereira, A. Mortadi, E.M. Sabbar, R. El Moznine, B. Sabour, Phycol. Res. 64 (2016) 185–193.
[45] Z. Belattmania, Thesis of Chouaib Doukkali University, El Jadida – Morocco, O.N. 295 (2018).
[46] S. El Atouani, Thesis of Chouaib Doukkali University, El Jadida – Morocco, O.N. 294 (2018).
[47] Z. Belattmania, A.H. Engelen, H. Pereira, E.A. Serrão, L. Custódio, J.C. Varela, R. Zrid, A. Reani, B. Sabour, Internat. Food Res. J. 25 (2018) 1520–1527.
[48] ASTM, G31-72, American Society for Testing and Materials, Philadelphia, PA, 1990.
[49] O. Olivares, N.V. Likhanova, B. Gómez, J. Navarrete, M.E. Llanos-Serrano, E. Arce, J.M. Hallen, Appl. Surf. Sci. 252 (2006) 2894–2909.
[50] M. Tourabi, K. Nohair, M. Traisnel, C. Jama, F. Bentiss, Corros. Sci. 75 (2013) 123–133.
[51] M. Lebrini, M. Lagrenée, H. Vezin, L. Gengembre, F. Bentiss, Corros. Sci. 47 (2005) 485–505.
[52] M.A. Quraishi, R. Sardar, Mater. Chem. Phys. 78 (2002) 425–431.
[53] M.A. Quraishi, M.A.W. Khan, M. Ajmal, S. Muralidharan, S.V. Iyer, Br. Corros. J. 32 (1997) 72–76.
[54] Y. Kharbach, F.Z. Qachchachi, A. Haoudi, M. Tourabi, A. Zarrouk, C. Jama, L.O. Olasunkanmi, E.E. Ebenso, F. Bentiss, J. Mol. Liq. 246 (2017) 302–316.
[55] J.O'M. Bockris, S. Srinivasan, Electrochim. Acta 9 (1964) 31–44.
[56] O. L. Riggs Jr., Corrosion Inhibition, second ed., C.C. Nathan, Houston, TX, 1973.
[57] I. Ahamad, M.A. Quraishi, Corros. Sci. 52 (2010) 651–656.
[58] M. Abdallah, Corros. Sci. 44 (2002) 717–728.
[59] I. Ahamad, R. Prasad, M.A. Quraishi, Corros. Sci. 52 (2010) 1472–1481.
[60] Z.B. Stoynov, B.M. Grafov, B. Savova-Stoynova, V.V. Elkin, Electrochemical Impedance; Nauka: Moscow, 1991.
[61] H. Shih, F. Mansfeld, Corros. Sci. 29 (1989) 1235–1240.
[62] I.D. Raistrick, D.R. Franceschetti, J.R. Macdonald, in: E. Barsoukov, J.R. Macdonald (Eds.), Impedance Spectroscopy, second ed., Theory, Experimental and Applications, John Wiley & Sons, New Jersey, 2005.
[63] R. Solmaz, G. Kardaş, M. Çulha, B. Yazıcı, M. Erbil, Electrochim. Acta 53 (2010) 5941–5952.
[64] A.K. Nigam, R. Balasubramaniam, S. Bhargava, R.G. Baligidad, Corros. Sci. 48 (2006) 1666–1678.
[65] M. ElBelghiti, Y. Karzazi, A. Dafali, B. Hammouti, F. Bentiss, I.B. Obot, I. Bahadur, E.E. Ebenso, J. Mol. Liq. 218 (2016) 281–293.
[66] B. Ramezanzadeh, S.Y. Arman, M. Mehdipour, B.P. Markhali, Appl. Surf. Sci. 289 (2014) 129–140.
[67] M. El Faydy, R. Touir, M. Ebn Touhami, A. Zarrouk, C. Jama, B. Lakhrissi, L.O. Olasunkanmi, E.E. Ebenso, F. Bentiss, Phys. Chem. Chem. Phys. 20 (2018) 20167–20187.
[68] L.O. Olasunkanmi, I.B. Obot, M.M. Kabanda, E.E. Ebenso, J. Phys. Chem. C 119 (2015) 16004–16019.
[69] A. Popova, M. Christov, Corros. Sci. 48 (2006) 3208–3221.
[70] A. Popova, M. Christov, A. Vasilev, Corros. Sci. 53 (2011) 1770–1777.
[71] C. Kamal, M.G. Sethuraman, Res. Chem. Intermed. 39 (2013) 3813–3828.
[72] C. Kamal, M.G. Sethuraman, Mater. Corros. 65 (2014) 846–854.
[73] M. Ramdani, H. Elmsellem, N. Elkhiati, B. Haloui, A. Aouniti, M. Ramdani, Z. Ghazi, A. Chetouani, B. Hammouti, Der Pharma Chemica 7 (2015) 67–76.

[74] D.K. Verma, F. Khan, I. Bahadur, M. Salmane, M.A. Quraishi, C. Verma, E.E. Ebenso. Results Phys. 10 (2018) 665–674.
[75] T. Benabbouha, M. Siniti, H. El Attari, K. Chefira, F. Chibi, R. Nmila, H. Rchid, J. Bio Tribo-Corros. 4 (2018) 39–45.
[76] C. Kamal, M.G. Sethuraman, Arab. J. Chem. 5 (2015) 155–161.
[77] R. Thilagavathi, A. Prithiba, R. Rajalakshmi, Orient. J. Chem. 35 (2019) 241–254.
[78] S.M. Shaban, I. Aiad, A.H. Moustafa, O.H. Aljoboury, J. Mol. Liq. 273 (2019) 164–176.
[79] M. Faustin, A. Maciuk, P. Salvin, C. Roos, M. Lebrini, Corros. Sci. 92 (2015) 287–300.
[80] J. de Damborenea, J.M. Bastidas, A.J. Vázquey, Electrochim. Acta 42 (1997) 455–459.
[81] M. Elayyachy, A. El Idrissi, B. Hammouti, Corros. Sci. 48 (2006) 2470–2479.
[82] F. Bentiss, M.Lebrini, H. Vezin, F. Chai, M. Traisnel, M. Lagrenée, Corros. Sci. 51 (2009) 2165–2173.
[83] M.J. Bahrami, S.M.A. Hosseini, P. Pilvar, Corros. Sci. 52 (2010) 2793–2803.
[84] A.K. Singh, M.A. Quraishi, Corros. Sci. 53 (2011) 1288–1297.
[85] M. Faustin, M. Lebrini, F. Robert, C. Roos, Int. J. Electrochem. Sci. 6 (2011) 4095–4113.
[86] M. Lebrini, F. Robert, C. Roos, Int. J. Electrochem. Sci. 6 (2011) 847–859.
[87] M. Faustin, A. Maciuk, P. Salvin C. Roos, M. Lebrini, Corros. Sci. 92 (2015) 287–300.
[88] N. El Hamdani, R. Fdil, M. Tourabi, C. Jama, F. Bentiss, Appl. Surf. Sci. 357 (2015) 1294–1305.
[89] G.P. Lopez, D.G. Castner, B.D. Ratner, Surf. Interf. Anal. 17 (1991) 267–272.
[90] W. Temesghen, P.M.A. Sherwood, Anal. Bioanal. Chem. 373 (2002) 601–608.
[91] S.K. Papageorgiou, E.P. Kouvelos, E.P. Favvas, A.A. Sapalidis, G.E. Romanos, F.K. Katsaros, Carbohyd. Res. 345 (2010) 469–473.
[92] K. Babić-Samardžija, C. Lupu, N. Hackerman, A.R. Barron, A. Luttge, Langmuir 21 (2005) 12187–12196.
[93] M. Bouanis, M. Tourabi, A. Nyassi, A. Zarrouk, C. Jama, F. Bentiss, Appl. Surf. Sci. 389 (2016) 952–966.
[94] P. Mourya, P. Singh, A.K. Tewari, R.B. Rastogi, M.M. Singh, Corros. Sci. 95 (2015) 71–87.
[95] M. Outirite, M. Lagrenée, M. Lebrini, M. Traisnel, C. Jama, H. Vezin, F. Bentiss, Electrochim. Acta 55 (2010) 1670–1681.
[96] A. Galtayries, R. Warocquier-Clérout, M.-D. Nagel, P. Marcus, Surf. Interface Anal. 38 (2006) 186–190.
[97] V.S. Sastri, M. Elboujdaini, J.R. Rown, J.R. Perumareddi, Corrosion 52 (1996) 447–452.

Figure captions

Fig. 1. Schematic presentation of the main biological molecules containing in *Sargassum muticum* extract.

Fig. 2. E_{ocp} vs. time for CS electrode in 1 M HCl with various concentrations of ESM at 303 K.

Fig. 3. Polarization curves of CS in 1 M HCl containing different concentrations of ESM at 303 K.

Fig. 4. Nyquist diagrams for CS in 1 M HCl containing different concentrations of ESM after 6 h of immersion time at 303 K.

Fig. 5. Bode (a- modulus and b- phase angle) diagrams for CS in 1 M HCl containing different concentrations of ESM after 6 h of immersion time at 303 K.

Fig. 6. Electrical equivalent circuit used for modelling the interface CS / 1 M HCl solution without and with addition ESM.

Fig. 7. EIS Nyquist (a) and Bode (b) diagrams for CS / 1 M HCl + 0.75 g/L of ESM interface: (−□−) experimental; (—) fitted data using structural model in Fig. 6.

Fig. 8. SEM micrographs of the CS surface: a) after being polished, b) after 6 h immersion in 1 M HCl and c) after 6 h immersion in 1 M HCl containing 1.5 g/L of ESM.

Fig. 9. Isotherm model plots for ESM adsorption on CS surface in 1 M HCl.

Fig. 10. XPS survey spectrum of ESM treated-CS in 1 M HCl.

Fig. 11. High-resolution X-ray photoelectron deconvoluted profiles of C 1s, O 1s and Fe $2p_{3/2}$ for ESM treated CS substrate.

Fig. 12. High-resolution X-ray photoelectron deconvoluted profile of C 1s and O 1s for a-ESM powder and b- ESM treated CS substrate in 1 M HCl.

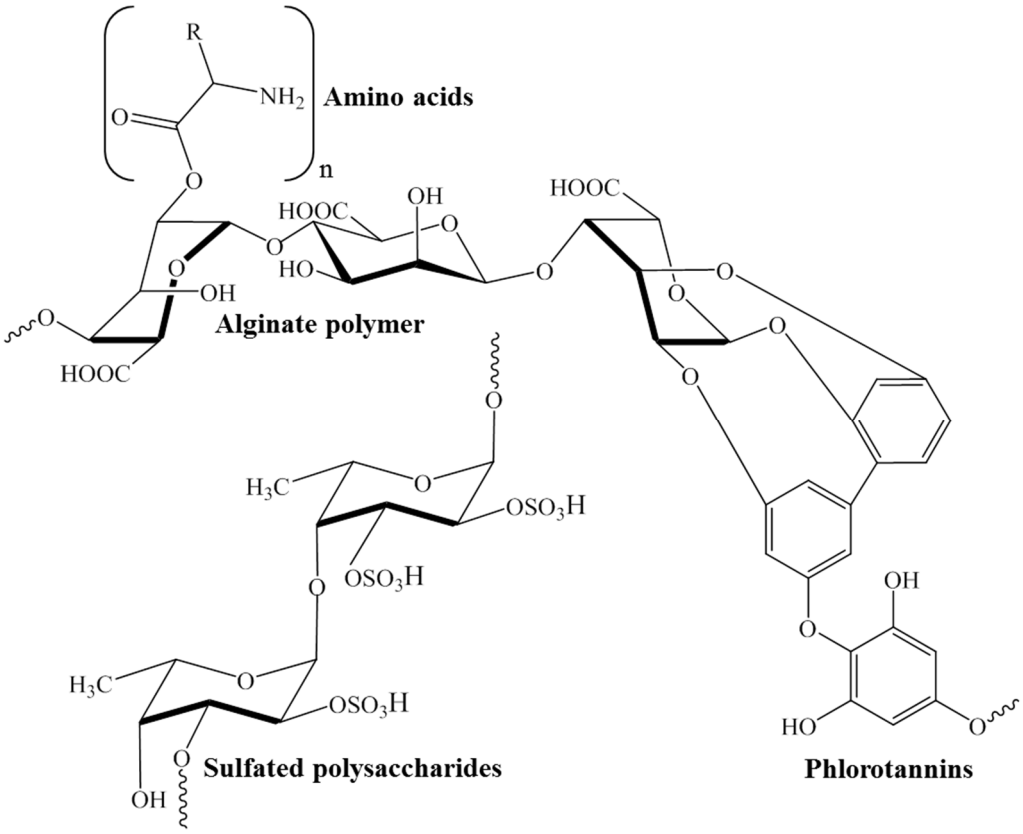
R
NH2
Amino acids
n
HOOC
OH
HO
OH
Alginate polymer
HOOC
H3C
OSO3H
OSO3H
H3C
OSO3H
OH
Sulfated polysaccharides
HOOC
OH
HO
Phlorotannins

Figure 1

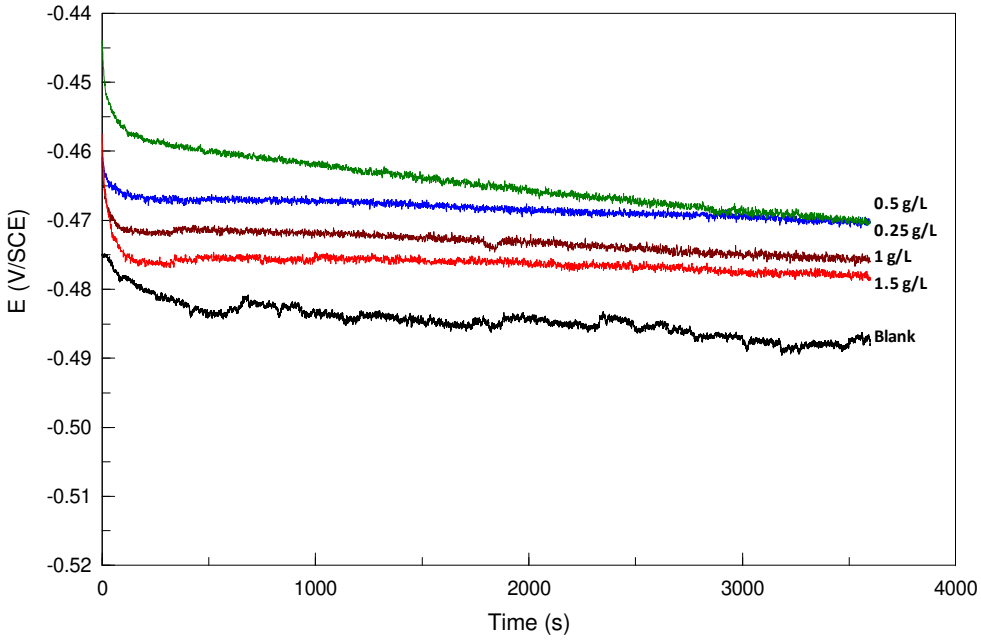
-0.44
-0.45
-0.46
-0.47
-0.48
-0.49
-0.50
-0.51
-0.52
E (V/SCE)
0
1000
2000
3000
4000
Time (s)
0.5 g/L
0.25 g/L
1 g/L
1.5 g/L
Blank

Figure 2

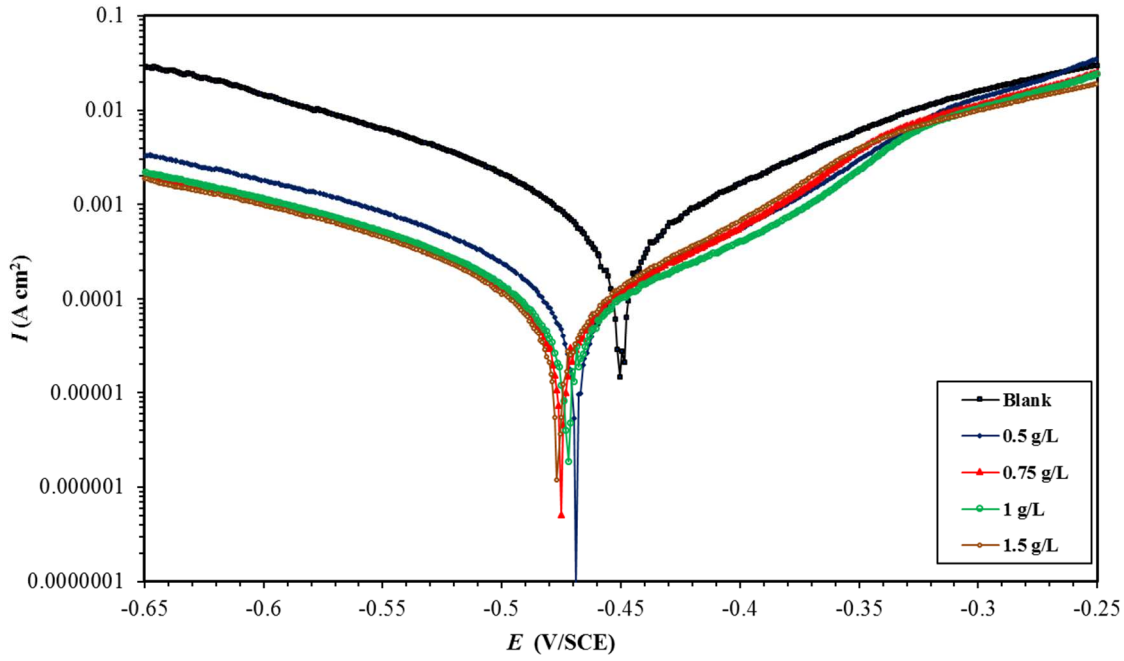
0.1
0.01
0.001
0.0001
0.00001
0.000001
0.0000001
I (A cm²)
-0.65
-0.6
-0.55
-0.5
-0.45
-0.4
-0.35
-0.3
-0.25
E (V/SCE)
Blank
0.5 g/L
0.75 g/L
1 g/L
1.5 g/L

Figure 3

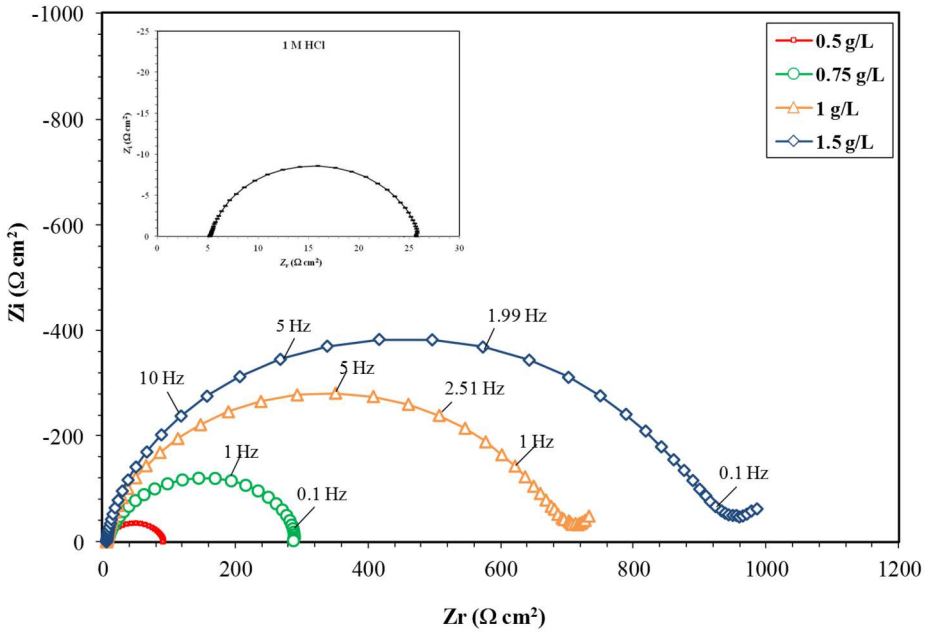
1 M HCl
0.5 g/L
0.75 g/L
1 g/L
1.5 g/L
5 Hz
1.99 Hz
10 Hz
5 Hz
2.51 Hz
1 Hz
1 Hz
0.1 Hz
0.1 Hz
Zi (Ω cm²)
Zr (Ω cm²)
-1000
-800
-600
-400
-200
0
0
200
400
600
800
1000
1200

Figure 4

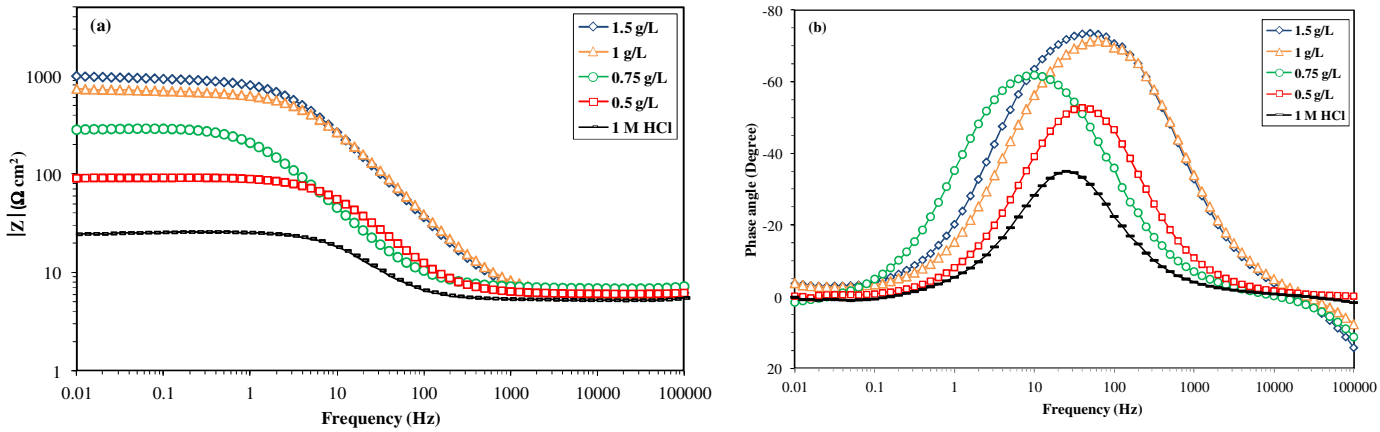
(a)
1.5 g/L
1 g/L
0.75 g/L
0.5 g/L
1 M HCl
|Z| (Ω cm²)
1000
100
10
1
0.01
0.1
1
10
100
1000
10000
100000
Frequency (Hz)
(b)
1.5 g/L
1 g/L
0.75 g/L
0.5 g/L
1 M HCl
Phase angle (Degree)
-80
-60
-40
-20
0
20
0.01
0.1
1
10
100
1000
10000
100000
Frequency (Hz)

Figure 5

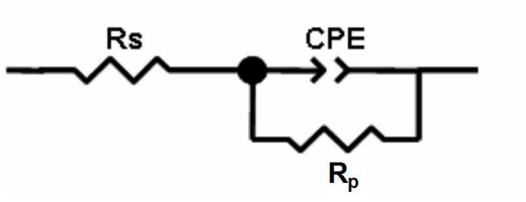

Figure 6

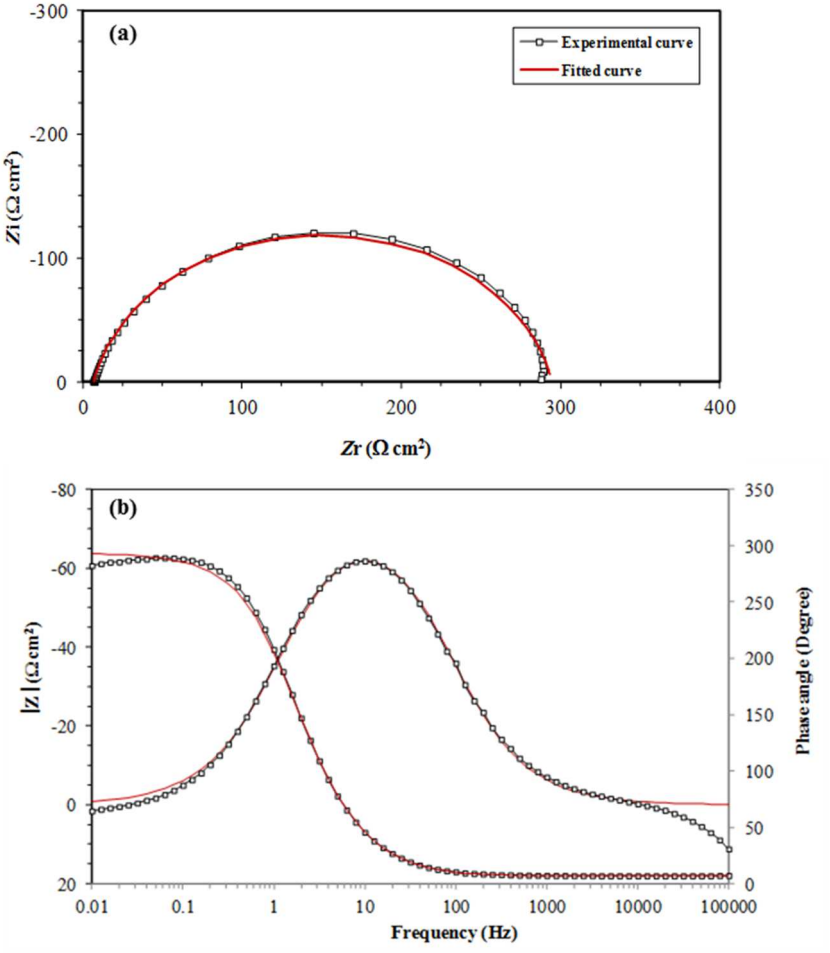
(a)
Experimental curve
Fitted curve
-300
-200
-100
0
Zi (Ω cm²)
0
100
200
300
400
Zr (Ω cm²)
(b)
-80
-60
-40
-20
0
20
|Z| (Ω cm²)
350
300
250
200
150
100
50
0
Phase angle (Degree)
0.01
0.1
1
10
100
1000
10000
100000
Frequency (Hz)

Figure 7

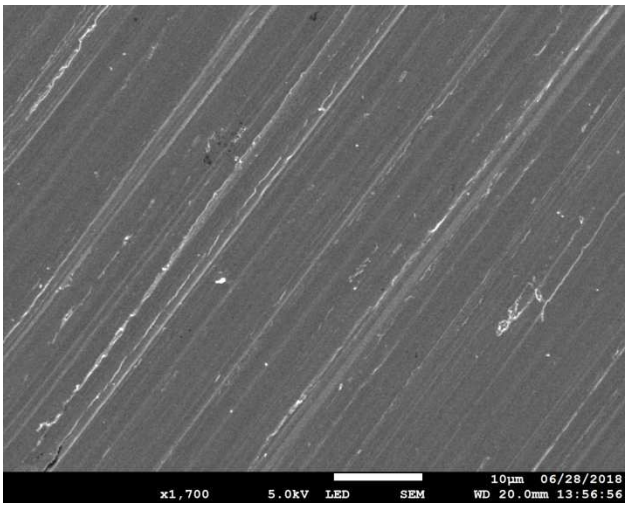
x1,700 5.0kV LED SEM 10µm 06/28/2018 WD 20.0mm 13:56:56

(a)

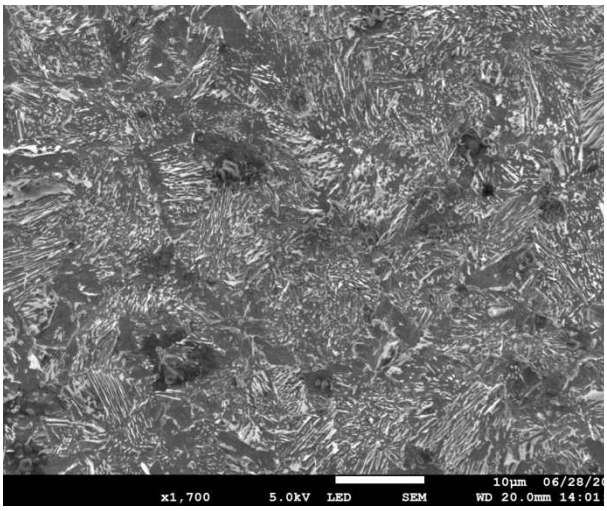
x1,700 5.0kV LED SEM WD 20.0mm 14:01

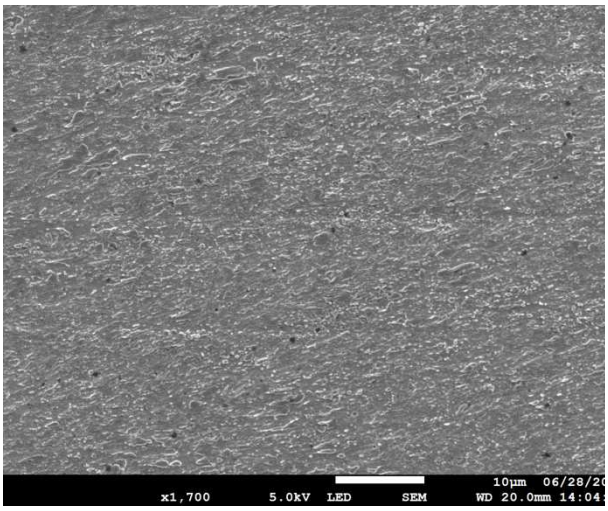
x1,700 5.0kV LED SEM 10µm 06/28/2

(b) **(c)**

Figure 8

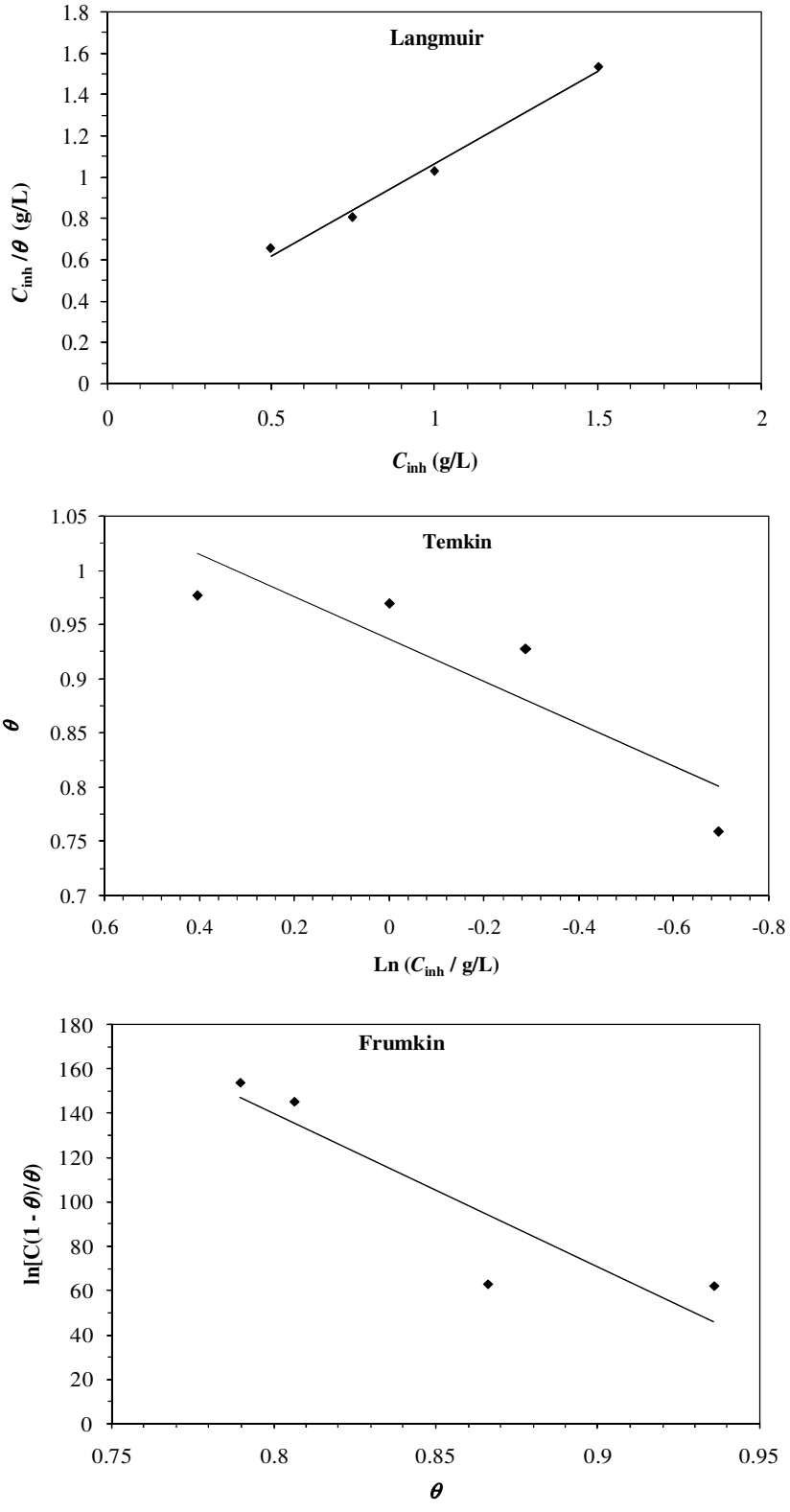
Langmuir
C_{inh} /θ (g/L)
C_{inh} (g/L)
Temkin
θ
Ln (C_{inh} / g/L)
Frumkin
ln[C(1 - θ)/θ]
θ

Figure 9

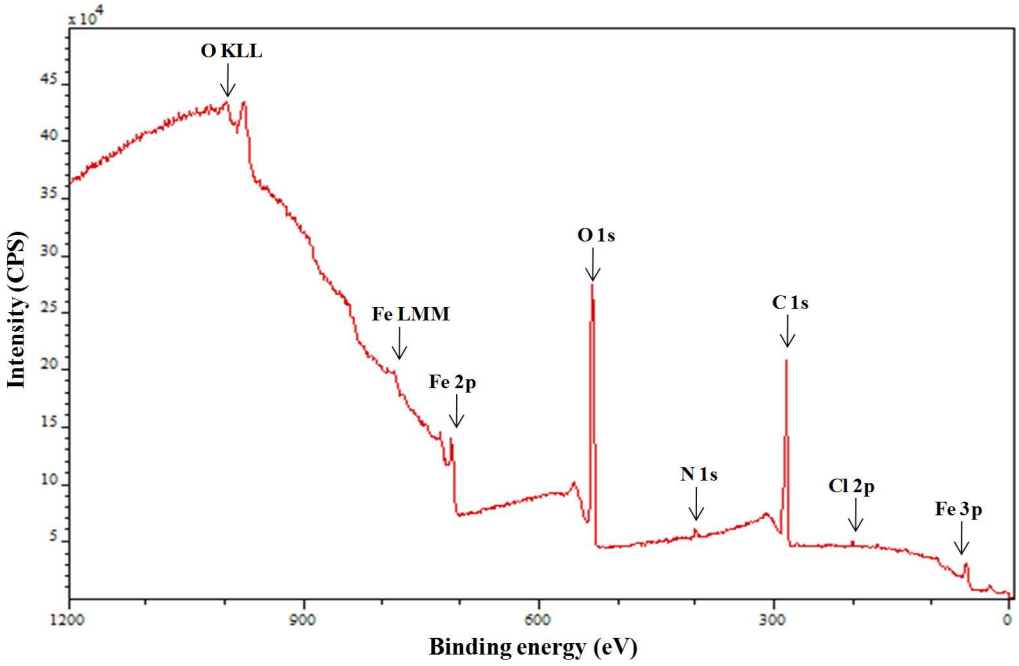
x 10^4
O KLL
Fe LMM
Fe 2p
O 1s
N 1s
C 1s
Cl 2p
Fe 3p
Intensity (CPS)
Binding energy (eV)
45
40
35
30
25
20
15
10
5
1200
900
600
300
0

Figure 10

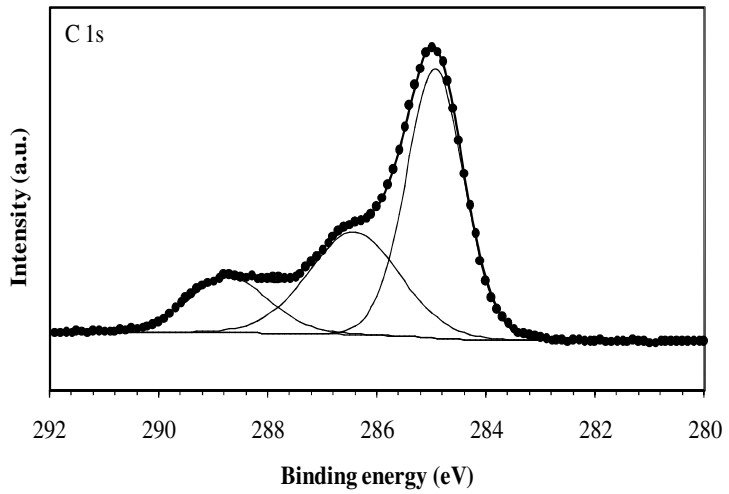
C 1s
Intensity (a.u.)
292
290
288
286
284
282
280
Binding energy (eV)

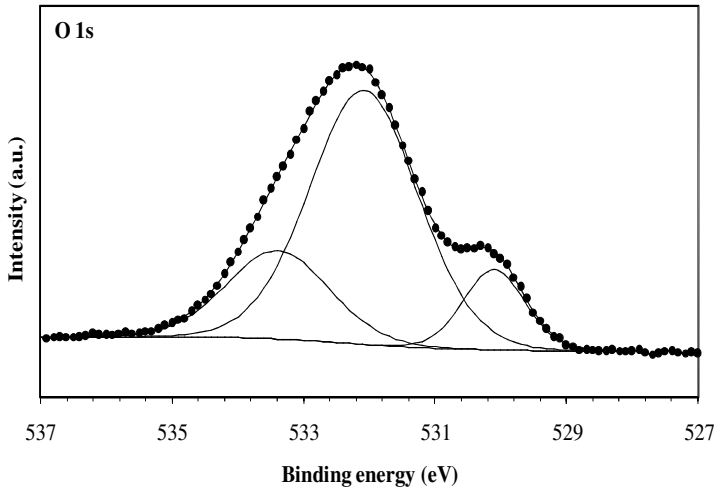
O 1s
Intensity (a.u.)
537
535
533
531
529
527
Binding energy (eV)

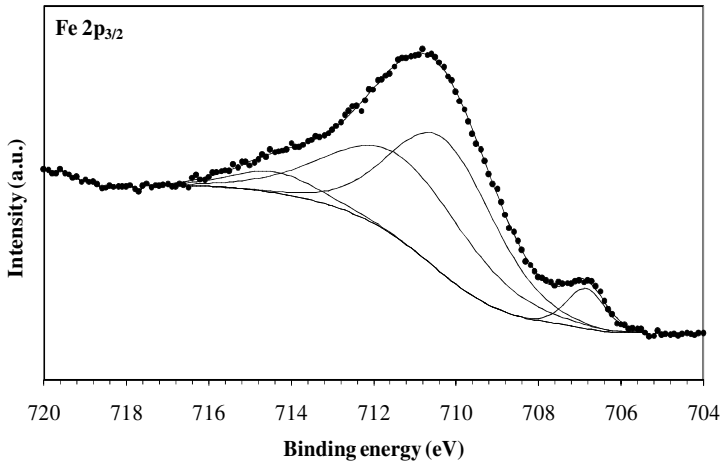
Fe 2p3/2
Intensity (a.u.)
720
718
716
714
712
710
708
706
704
Binding energy (eV)

Figure 11

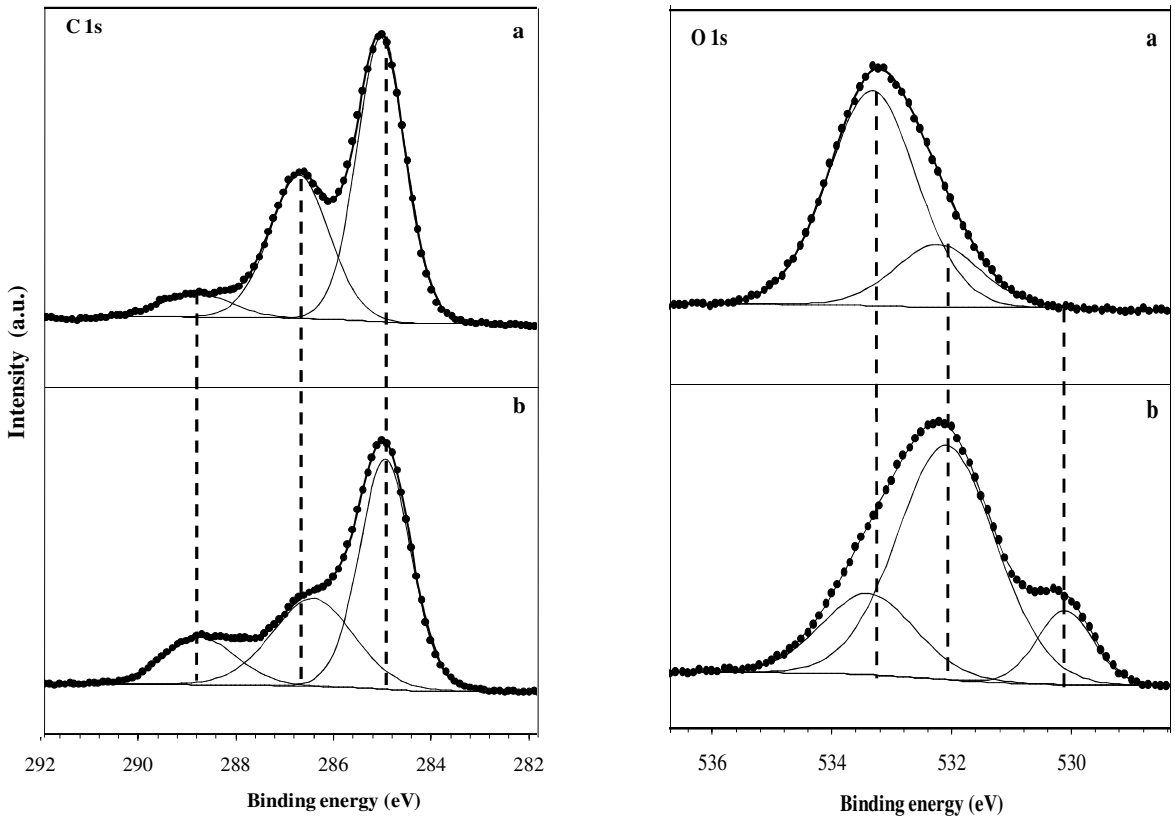
C 1s
a
b
Intensity (a.u.)
292
290
288
286
284
282
Binding energy (eV)
O 1s
a
b
536
534
532
530
Binding energy (eV)

Figure 12

Table 1

Weight loss parameters for CS corrosion in 1 M HCl containing various concentrations of ESM at 303 K.

Concentration (g/L)	C_R (10^3 mpy)	η_{WL} (%)
Blank	0.466 ± 0.002	—
0.5	0.123 ± 0.001	73.6 ± 0.3
0.75	0.087 ± 0.001	81.2 ± 0.2
1	0.024 ± 0.001	94.8 ± 0.2
1.5	0.016 ± 0.001	96.6 ± 0.1

Table 2

Polarization data of CS in 1 M HCl containing different concentration of ESM at 303 K.

Concentration (g/L)	$-E_{corr}$ (mV *vs* SCE)	$-\beta_c$ (mV dec^{-1})	β_a (mV dec^{-1})	i_{corr} (μA cm^{-2})	η_{Tafel} (%)
Blank	450	134 ± 4	98 ± 3	717 ± 12	—
0.5	470	115 ± 2	96 ± 3	161 ± 4	77.5
0.75	475	110 ± 3	93 ± 3	97 ± 4	86.4
1	472	100 ± 2	89 ± 3	80 ± 3	88.8
1.5	477	94 ± 2	86 ± 2	65 ± 2	90.9

Table 3

Impedance data for CS after 6 h immersion period in 1 M HCl containing different concentrations of ESM at 303 K.

Conc. (g/L)	R_s (Ω cm^2)	R_p (Ω cm^2)	$10^4 \times Q$ (Ω^{-1} s^n cm^{-2})	n	C_{dl} (μF cm^{-2})	τ (ms)	χ^2	η_Z(%)
Blank	5.87 ± 0.02	20.7 ± 0.1	4.22 ± 0.11	0.821 ± 0.006	150.1	3.1	4.31×10^{-4}	—
0.5	6.02 ± 0.02	85.9 ± 0.3	2.53 ± 0.04	0.879 ± 0.001	149.3	12.8	3.47×10^{-4}	75.9
0.75	6.89 ± 0.03	285.3 ± 1.6	2.06 ± 0.06	0.890 ± 0.001	145.2	41.4	6.39×10^{-4}	92.7
1	5.87 ± 0.02	676.6 ± 2.3	0.85 ± 0.03	0.902 ± 0.001	62.4	42.2	6.64×10^{-4}	96.9
1.5	5.83 ± 0.03	905.3 ± 4.5	0.78 ± 0.08	0.910 ± 0.002	61.6	55.7	3.87×10^{-4}	97.7

Table 4

Comparison of inhibition efficiency of *Sargassum muticum* extract (ESM) with available literature data of some algal extracts and alginate based polymers used as corrosion inhibitors for steel in HCl medium.

Compound	HCl concentration (M)	Optimum concentration	Immersion time (h)	Temperature (K)	Type of steel	Inhibition efficiency [(a)] (%)
Crude algal extract (natural inhibitor)						
Hydroclathrus clathratus [71]	1	0.5 g/L	0.5	303	Mild steel	65.28
Kappaphycus alvarezii [72]	1	0.5 g/L	0.5	303	Mild steel	69.33
Caulerpa prolifera [73]	1	1 g/L	0.5	308	Mild steel	94.72
spirogyra [74]	1	2 g/L	0.5	298	Mild steel	67.15
Halopitys incurvus [75]	1	0.6 g/L	0.5	298	Carbon steel	81.86
Spirulina platensis [76]	1	0.5 g/L	0.5	303	Mild steel	75.82
Sargassum polycystum [77]	1	0.7 (%v/v)	0.5	303	Mild steel	93.6
Sargassum muticum [this work]	1	1 g/L	6	303	Carbon steel	96.9
Alginate based polymers (synthetic inhibitor)						
ALGOB [78]	0.5	1 g/L	0.5	298	Mild steel	74.45
ALGDB [78]	0.5	1 g/L	0.5	298	Mild steel	78.44
ALGHB [78]	0.5	1 g/L	0.5	298	Mild steel	83.29
AS [35]	1	5×10^{-3} M	1	298	Carbon steel	92.90
AS-Zn [35]	1	5×10^{-3} M	1	298	Carbon steel	94.11
AS-Co [35]	1	5×10^{-3} M	1	298	Carbon steel	95.34
AS-Cu [35]	1	5×10^{-3} M	1	298	Carbon steel	96.27
HPA [36]	1	0.5 g/L	0.5	298	Mild steel	83.5

[(a)] The inhibition efficiency values were determined using AC impedance measurements

Table 5

Binding energies (eV), relative intensity and their assignment for the major core lines observed of ESM treated CS substrate.

Element	Position (eV)	Assignment
C 1s	285.0 (53 %)	C–H / C–C / C=C
	286.4 (32 %)	C–O / C–N / O=C–O^-
	288.7 (15 %)	O=C–O^-, π-π* shakeup satellite
O 1s	530.1 (12 %)	O^{2-} in Fe_2O_3
	532.1 (66 %)	OH^- in FeOOH / C–O / O=C–O^-
	533.4 (22 %)	O=C–O^- / H_2O_{ads}
Fe $2p_{3/2}$	706.8 (5 %)	Fe^0
	710.3 (49 %)	Fe_2O_3 and FeOOH
	711.3 (40 %)	FeOOH
	714.4 (6 %)	$FeCl_3$ and / or satellite of Fe^{3+}

Table 6

Surface elemental concentrations (% At.) in ESM powder and ESM treated-steel

Element	ESM powder	ESM treated-steel
C	68.01	68.75
O	21.03	27.86
N	1.02	1.12
Cl	5.84	0.34
Fe	—	1.93
Mg	3.58	—
S	0.57	—